INTEGR. COMP. BIOL., 42:988–996 (2002)

The Scaling and Structure of Aquatic Animal Wakes[1]

JOHN J. VIDELER,[2] EIZE J. STAMHUIS, ULRIKE K. MÜLLER,[3] AND LUCA A. VAN DUREN[4]
Department of Marine Biology, University of Groningen, P.O. Box 14, 9751 AA Haren, The Netherlands

SYNOPSIS. Animal generated water movements are visualized and quantified using two-dimensional particle image velocimetry (PIV). The resulting vector flow fields allow for the study of the distribution of velocity, vorticity and vortices. Structural and temporal aspects of animal-induced flows covering a range of Reynolds (*Re*) numbers between less than 1 to more than 10^4 are presented.

Maps of flow induced by continuous foraging and intermittent escape responses of tethered nauplius and copepodid stages of the marine copepod *Temora longicornis* offer insight in viscosity-dominated flow regimes. Fast escape responses of the equally sized largest nauplius stage and the smallest copepodid stage are compared. The nauplius moves by generating a viscous flow pattern with high velocities and vorticity; the copepodid moves by using inertial effects to produce a vortex ring with a rearward jet through the center.

Larvae and small adult fish (zebra danio) use a burst-and-coast-swimming mode at *Re* numbers up to 6,000, shedding a vortex ring with the associated jet at the tail during the burst phase. Flow patterns during the coasting phase differ between the small larvae and larger adults due to the changes in importance of viscosity.

A 12 cm long mullet swimming in a continuous mode generates a chain of vortex rings with a backward undulating jet through the centers of the rings at *Re* numbers of 4×10^4 in inertia-dominated regimes.

Our empirical results provide realistic insight in the scale effects determining the morphology of the interactions between animals and water.

INTRODUCTION

Moving aquatic animals exchange forces with the fluid. Every force exerted by the animal is opposed by an equal reaction force in opposite direction according to Newton's third law. Moving in a fluid is complicated by the fact that forces applied to the medium cause it to move.

Water can be considered an incompressible fluid with a density (ρ) of about 10^3 kg m^{-3} for fresh water at 1 atm and 15°C and a viscosity (μ) of about 10^{-3} (Pas or Nsm^{-2}). The amount of moving water and the speed and direction of movement in reaction to the propelling animal depends on the size of the propeller and the speed of its movement. This movement is characterized by the non-dimensional Reynolds number (*Re*), which is the ratio of the product of speed u (m s^{-1}) and length 1 (m) and the kinematic viscosity ν (m^2 sec^{-1}) (Reynolds, 1883). The kinematic viscosity is the ratio of viscosity over density. *Re* is usually expressed as:

$$Re = \mathrm{ul}\ \rho\mu^{-1}$$

At a given kinematic viscosity, the *Re* number will, by definition, scale with speed and length. The range for animals starts with values less than one for protozoans and ends with figures reaching 10^8 for the blue whale. Figure 1 relates typical swimming speeds of aquatic organisms with the *Re* number based on these speeds and the body lengths (note the logarithmic scales). The relative importance of viscosity and inertia over the range of *Re* number regimes is indicated below the graph. There is a zone of overlap where both viscosity and density reign. At low *Re* numbers, the flow caused by animal movements is dominated by viscous forces. This implies a lack of continuation of the flow phenomena after the movements that caused them stops. The flow will have the tendency to remain laminar at low *Re* numbers but rotation is not precluded by the mainly viscous nature of the interaction among water particles. Rotational flow is the predominant type of flow. Shear due to friction in the fluid will soon stop the movements and the energy will dissipate as heat.

In a fluid medium, generation of velocity gradients usually induces rotational movements or vortices. A vortex has a centre where the rotational velocity is minimal; away from the centre the rotational velocity increases to a maximum and gradually dies out beyond that. The rate of rotation is termed vorticity, which is usually maximal in the centre of a vortex. Fluid dynamic theory implies that, in the direction along its centre, a vortex cannot end in the fluid. A vortex may either end at the boundary of the fluid or may form a closed loop with itself to form a vortex ring (Lighthill, 1986). This is important in the present work as movements of animals generate velocity gradients and hence vortices.

At the inertia-dominated end of the *Re* scale, movement causes turbulence in the water. Vortices form and break up readily and make the flow highly unstructured. Inertia is the dominant physical factor and the fluid keeps moving long after the causes have ceased to exist. In intermediate *Re* ranges, both viscosity and

[1] From the Symposium *Dynamics and Energetics of Animal Swimming and Flying* presented at the Annual Meeting of the Society for Integrative and Comparative Biology, 2–6 January 2002, at Anaheim, California.

[2] E-mail: j.j.videler@biol.rug.nl

[3] Present address of U.K. Müller is: Department of Zoology, Cambridge University, Downing Street, Cambridge, CB2 3EJ, UK.

[4] Present address of L.A. van Duren is: Netherlands Institute of Ecology, P.O. Box 140, 4400 AC Yerseke, The Netherlands.

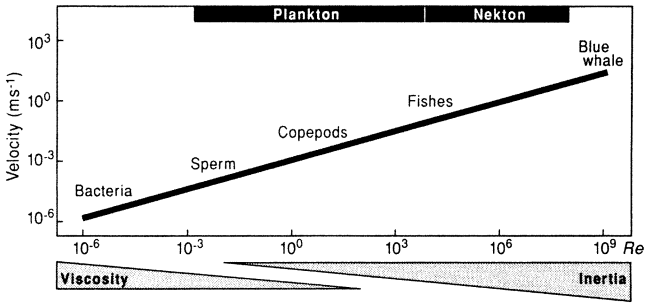

FIG. 1. Typical velocities of the largest possible size range of swimming organisms as a function of the *Re* number (From Videler, 1993).

inertia determine the flow patterns. It is hard to predict from hydrodynamic theory what kind of patterns can be expected. Under this regime, vortices can be either laminar or turbulent.

A vortex ring consists of a circle of rotating fluid with a jet through the centre (See Fig. 2a). Vortex rings may interact with each other to form more complex 3-D fluid structures. A schematic representation of the flow structures in a chain of three vertical vortex rings is shown as an example in Figure 2b. The rotations of the vortex rings generate a jet which undulates through the centres of the rings.

Quantitative studies of animal-generated flow at a large range of *Re* numbers have hardly been made. The techniques to do so only recently became available to biologists interested in the interactions between animals and water.

In this study we present quantitative data collected of animal-induced flow phenomena covering a *Re* number range from less than 1 to well over 10^4. Water movements in the wakes of foraging and swimming animals are sampled by analyzing the displacements in time of particles in a thin sheet of laser light. Particle image velocimetry (PIV) and particle tracking velocimetry (PTV) were used to quantify the flow fields (Stamhuis and Videler, 1995).

Flow induced by foraging and escape responses of tethered nauplius and copepodid stages of *Temora longicornis* offers insight in viscosity-dominated flow regimes at *Re* numbers ranging from 0.1 to 100 (Van Duren, 2000). Coasting and swimming larvae of free-swimming zebra danio's (*Brachidanio rerio*) represent *Re* regimes between 100 and 5,000. Twelve cm long mullets (*Chelon labrosus*) swimming at 1.4 body length sec^{-1} reach *Re* values of 2×10^4, placing them well into inertia-dominated flow regimes.

We will compare and discuss both structural and temporal aspects of the range of flow patterns found. More detailed accounts of the flow phenomena generated by copepod stages and fish larvae and adults can be found in Van Duren and Videler (submitted), Van Duren (2000) and in Müller *et al.* (1997, 2000, 2001) respectively. Here we will restrict ourselves to examples from our studies showing the changes in the interactions between animals and water for a large

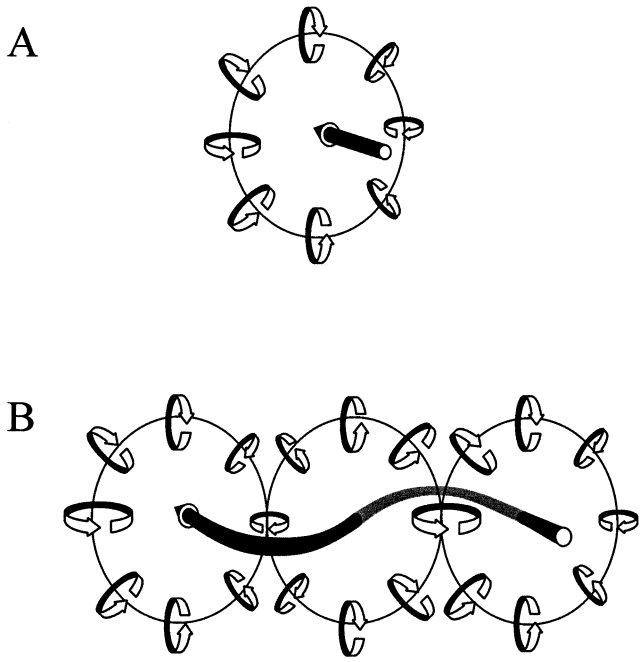

FIG. 2. Schematic drawings of vortex ring structures. A. A single vortex ring. The ring shaped centre of rotation is drawn as a line. Rotations of the vortex ring structure draw a jet of water through the centre of the ring. B. An artist impression of a chain of three connected vortex rings. A resulting jet of fluid undulates through the centres of the vortex rings building the chain.

range of *Re* numbers. It is an interesting range because both viscous and inertial forces are clearly influential in different ways for various *Re* numbers and theoretical predictions of what can be expected are difficult to make.

It is our aim to provide some practical feeling for animal-generated flows to accommodate zoologists with a general interest in these phenomena. Computational fluid dynamicists can use the empirical data to verify their predictions regarding shape and time span of animal-induced flows.

METHODS

Experimental animals

The calanoid copepod *Temora longicornis* (Müller) was cultured in the laboratory. The life cycle includes 12 stages: 6 nauplius (N1 to N6) and 6 copepodid stages (C1 to C6). C6 is the adult stage with a carapace length of around 1 mm (see Fig. 3). The shape of the body differs considerably between nauplii and copepodids. The change from a globular nauplius with 3 pairs of appendages to the streamlined adult shape occurs when N6 moults into C1. The animals were tethered to the tip of a very thinly drawn glass pipette using a suction restraint technique. The tip of the pipette was connected to the dorsal side of the carapace. Examples of flow fields during routine feeding movements and escape responses of nauplii and copepodids due to light-pulsing are included in this study (Van Duren, 2000).

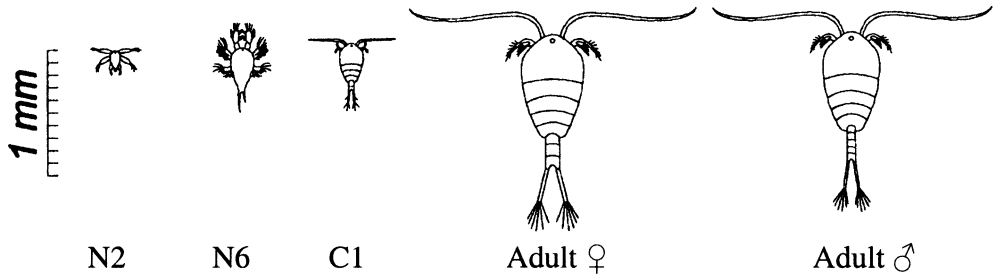

FIG. 3. Developmental stages of the calanoid copepod *Temora longicornis* (Müller).

Zebra danio larvae of 4 mm body length and 35 mm long adults use the same burst and coast swimming style (Fuiman and Webb, 1988). The experiments on the larvae were conducted in a $60 \times 60 \times 50$ mm^3 transparent Perspex container holding 5 free-swimming larvae at a time to increase the chances of obtaining results. Single adults were studied in a $300 \times 150 \times 150$ mm^3 glass tank (see Müller *et al.*, 2000 for details).

We include data of a steady swimming 12 cm long thick-lipped mullet. A $1.5 \times 0.3 \times 0.5$ m^3 test aquarium was used to record the wake caused by the swimming movements (details of the experiment are in Müller *et al.*, 1997).

Flow visualization and characterization

The animals move in particle-seeded water. Neutrally buoyant particles varied in diameter between 4 and 200 μm depending on the size of the experimental animal. We used nylon beads of 4 μm (TSI Inc.), Pliolite particles of 50 μm (BASF) and unexpanded polystyrene particles varying in size between 25 and 200 μm. A red krypton laser beam was turned into a thin light sheet by a cylindrical lens. A video camera mounted normal to the light sheet recorded the movements of the particles. Details of the methods are described in Stamhuis and Videler (1995). The flow analysis technique derives velocity vectors from particle positions in two successive frames. The choice of time resolution depends on the flow velocities. The displacement of a particle or a group of particles in a given time provides an estimate of the local speed and direction of the flow. The velocity vectors in an orthogonal frame of reference are used to calculate derived characteristic features of the flow used in the comparison of the flow at different *Re* regimes. Therefore each velocity vector is resolved in a component **u** in the x-direction and a component **v** in the y-direction. Partial derivatives can be obtained by numerical differentiation of **u** and **v** in the x and y directions. These can be used to calculate vorticity (ω), describing the rate of rotation of the fluid as:

$$\omega = \partial \mathbf{v}/\partial x - \partial \mathbf{u}/\partial y$$

Note that the unit of this parameter is sec^{-1}. In the following sections, data is presented using absolute velocities in mm sec^{-1}, velocities relative to the body in body-lengths sec^{-1} (L sec^{-1}), and vorticity in sec^{-1}.

RESULTS

Foraging copepod stages: 0.1 < Re < 5

Feeding copepods generate currents that propel the animal, thus drawing food in the direction of their mouth. Stationary suction tethered animals move water relative to their position. Under these conditions we compare velocity vector fields during foraging of nauplius stage N6 with those of copepodid C1. N6 is 0.35 mm and C1 0.33 mm long. Both horizontal and vertical light sheets are used to obtain an impression of the 3-D nature of the flow. Examples are shown in Figure 4 where the arrows show the direction and velocity of the flow. The maximum velocities for both instars range between 0.8 and 1.4 mm sec^{-1} (2.3 and 4.2 L sec^{-1}). The *Re* numbers of 0.2 and 0.4 are based on the maximum velocities and on the lengths of the animals. The vertical sheets show that the maximum velocities are reached underneath the animals at the approximate position of the moving appendages. In both cases the water changes direction in the region with the highest velocities. The maximum vorticity is similar for N6 and C1, reaching values near 4.5 sec^{-1}. The vorticity and velocity maxima coincide. Note that there are no clear vortices. The *Re* number during routine foraging ranges from 0.1 for the smallest foraging stage N2 to values well over 4 for the adult stage C6.

Escape responses of N6 (Re = 2) and C1 (Re = 7) compared

For our scaling purpose we choose examples from escape responses of a nauplius larva N6 and a copepodid C1. Both animals were 0.35 mm long. This figure is used in the *Re* number calculations. During foraging, the flow patterns of N6 and C1 are remarkably similar. The ranges of maximum escape speeds found are also very similar (Van Duren, 2000). Only when studying the nature of the flow during escape behavior did differences become apparent. The examples shown in Figure 5 are chosen to illustrate these differences. In Figure 5 the arrows indicating speed and direction of the local flow show clockwise and counter-clockwise rotation. At the peak of the escape burst of N6 water velocities reach maximum values of 5 mm sec^{-1} (14 L sec^{-1}) near the moving appendages. There is a clockwise vorticity maximum of >20 sec^{-1} in the same area. Counter-clockwise vorticity above the animal is more diffuse and shows up very weak. The water is drawn from

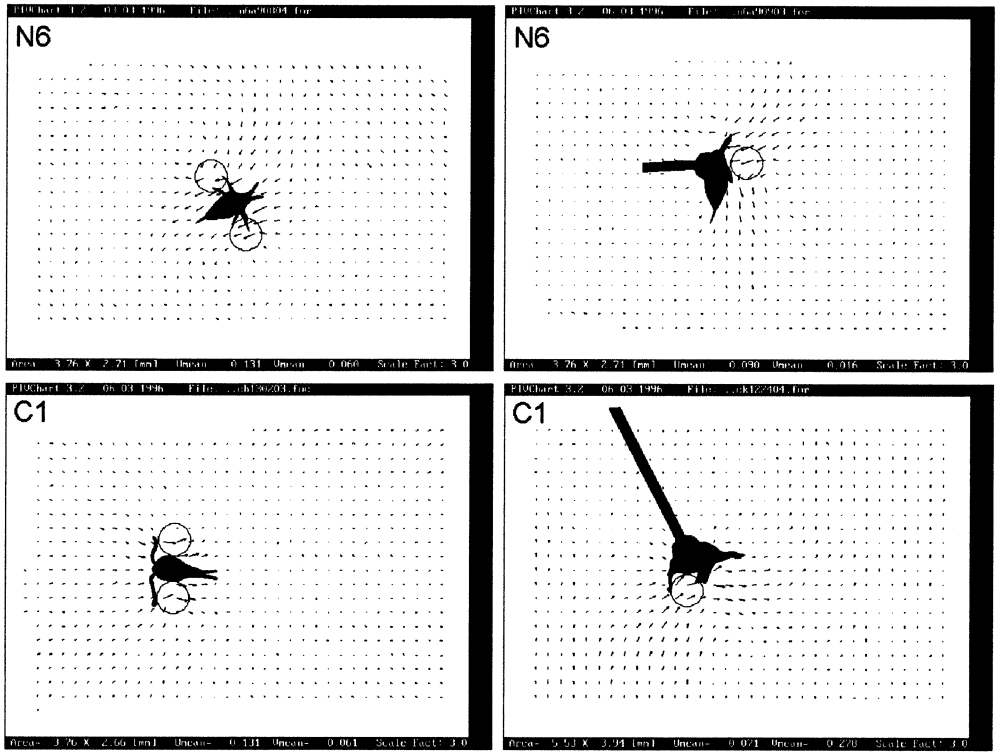

FIG. 4. Velocity fields around foraging nauplius (N6) and copepodid (C1) larvae of *Temora longicornis*. The panels on the left show the flow in a horizontal, those on the right in a vertical laser sheet. The black arrows indicate the speed and the direction of the flow, circles are drawn around areas with maximum vorticity. See text for further explanation.

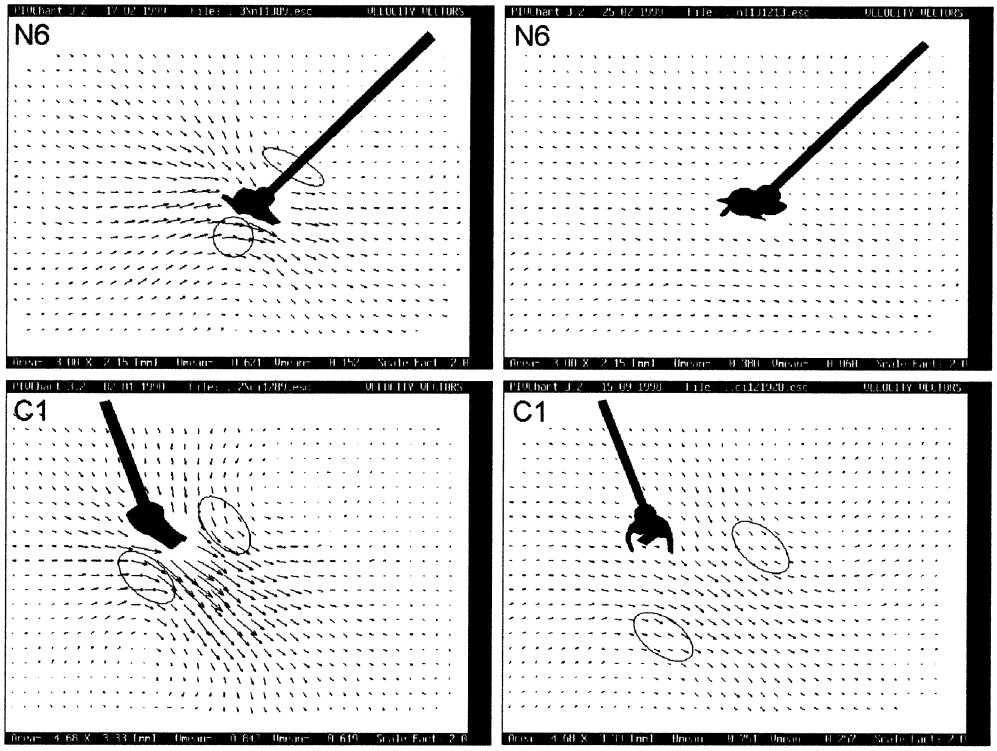

FIG. 5. Flow patterns around escaping nauplius (N6) and copepodid (C1) stages of *Temora longicornis*. The panels on the left show velocities (black arrows) and vorticity maxima (circles) at the peak of the escape movement. The right hand panels present the same parameters 0.06 sec after cessation of the leg movements.

below in front of the animal and is moving downward at the rear. The *Re* number is about 2. The peak escape movements of C1 generate water velocities of up to 21 mm sec^{-1} (60 L sec^{-1}). These maxima are found somewhat to the rear of the animal. There are two clear vorticity maxima reaching values of 27.7 sec^{-1}. The vector field represents a vertical section through a vortex ring. The rotational flow in the upper cross section of the ring is counter clockwise, that in the lower cross-section clockwise. There is a clear rearward jet through the center of the ring. The *Re* number at which these flow phenomena occur is about 7.

The right hand panels of Figure 5 show the flow fields 0.06 s after cessation of the leg movements. Velocities already decreased dramatically and vorticity disappeared almost instantly under *Re* = 2 regime of N6, showing that viscosity dominates. At Re = 7 in the C1 case inertial effects are apparent. The vortex ring structure with its jet through the center is clearly shifted away from the animal. Maximum vorticity decreased from 27.7 to 4.3 sec^{-1}. Velocities in the jet are about 30% of the maximum values at the peak of the escape movement. Although the vortex ring structure disappears within 0.15 sec, a clear effect in the structure of the velocity field is measurable up to 0.4 sec after cessation of the leg movements.

The decrease of viscous effects with increasing Re number

Coasting zebra danio larvae and adults are used here to exemplify flow phenomena with decreasing *Re* numbers (data are taken from Müller *et al.*, 2000). Both larvae and adults of this fish species use a burst-and-coast swimming style. In the context of our survey the coasting phase is particularly interesting. The animal stops the body and tail movements of the burst and glides with a stretched body to a halt (larvae) or until it starts the next burst (adults). The forces between the coasting animals and water are drag forces. Figure 6 (A, B) shows the velocity vectors and the maximum vorticity value at two instances during a larval glide 0.16 and 0.48 sec after the initiation of the burst. The initial coasting velocity of the 4.1 mm long larva is 40 mm sec^{-1} (10 L sec^{-1}), the *Re* number at that speed is 160. There is a large body of water around the larva at t = 0.16 sec moving on average in the same direction. The larva coasts at 5.7 mm sec^{-1} (1.4 L sec^{-1}) in the center of a large vortex ring. The vector field shows a section through this ring with a clockwise rotating vortex on the right and a counter clockwise rotating one on the left. The *Re* number is already reduced to about 23. The maximum vorticity is 6.38 sec^{-1}. At t = 0.48 sec the maximum vorticity found around the larva is down to 1.34 sec^{-1}. The speed is reduced to 0.5 mm sec^{-1} (0.12 L sec^{-1}) and the *Re* number to 2. The diameter of the vortex forming the ring has increased showing the dissipation due to viscous effects. The total distance covered to stand still when coasting with a straight body was 0.4 mm, which is 0.1 times its body length.

The picture of the flow field around a coasting 35 mm long adult (Fig. 6C) was taken 0.4 sec after the start of the tail flick. The maximum speed of 176 mm sec^{-1} (5 L sec^{-1}) is at this instant reduced to 81 mm sec^{-1} (2.3 L sec^{-1}) and the *Re* number went down from more than 6,000 to less than 3,000. The flow phenomena differ dramatically from those around the coasting larva. We see some water being pushed away by the head, but otherwise no water seems to be dragged along by the gliding body. There is some vorticity on each side of the body, revealing remaining viscous effects, but most of it can be found in the wake behind the body with a maximum value of 0.92 sec^{-1}, which is even less than the value found for the larva coasting at 0.5 mm sec^{-1}. A rough estimate of the distance it would cover to stand still is one body length.

The structure and fate of the flow caused by the tail flick of a fish larva

A 4.1 mm long zebra danio larva is shown in Figure 7A at t = 0 sec at the instant of the tail flick. The larva disappears in the direction of the arrow. The estimated initial velocity is about 100 mm sec^{-1} (24 L sec^{-1}) at a *Re* number of 400. Figure 7B shows a horizontal section through the resulting flow pattern at t = 0.24 sec. The arrows indicate the direction and velocity of the water and the maximum vorticity is indicated. In the lower left corner water flows in the direction where the larva disappeared. The vorticity there is part of the bound vortex around the larva that we saw in the previous paragraph. The tail flick produced a jet with an associated vortex ring showing up as a vortex pair. A jet through the center of the ring has a mean speed of 3.7 mm sec^{-1}. The jet and the vortex ring are the flow structures left behind by the escaping animal. The diameter of the ring has approximately the size of the length of the larva. The maximum vorticity at t = 0.24 sec is 9.25 sec^{-1}. At t = 0.64 sec (Fig. 7C) the vortex has grown in size and the peak vorticity is reduced to 2.56 sec^{-1}. The vorticity will disappear entirely in less than 1 sec due to viscous dissipation.

The wake behind a steadily swimming mullet at Re = 2×10^4

The 12.6 cm long mullet cruised steadily at 17.5 cm sec^{-1} (1.4 L sec^{-1}) across the field of view of the camera along a straight track at constant depth from right to left. The horizontal laser light sheet illuminating the particles coincided with the medio-frontal plane through the fish. Figure 8A–C are a time sequence with 0.16 sec intervals showing the flow velocity vector fields as black arrows. In Figure 8A the rear part of the fish is still visible. There are two vortex pairs present in the field of view. One more pair has been shed by the beating tail at t = 0.16 sec when the tail tip leaves the area to the left in Figure 8B. Vortices numbered 1 and 3 rotate counter clockwise, 2 and 4 clockwise. A jet of water undulates between the successive vortices. At t = 0.32 sec the wake is still clear-

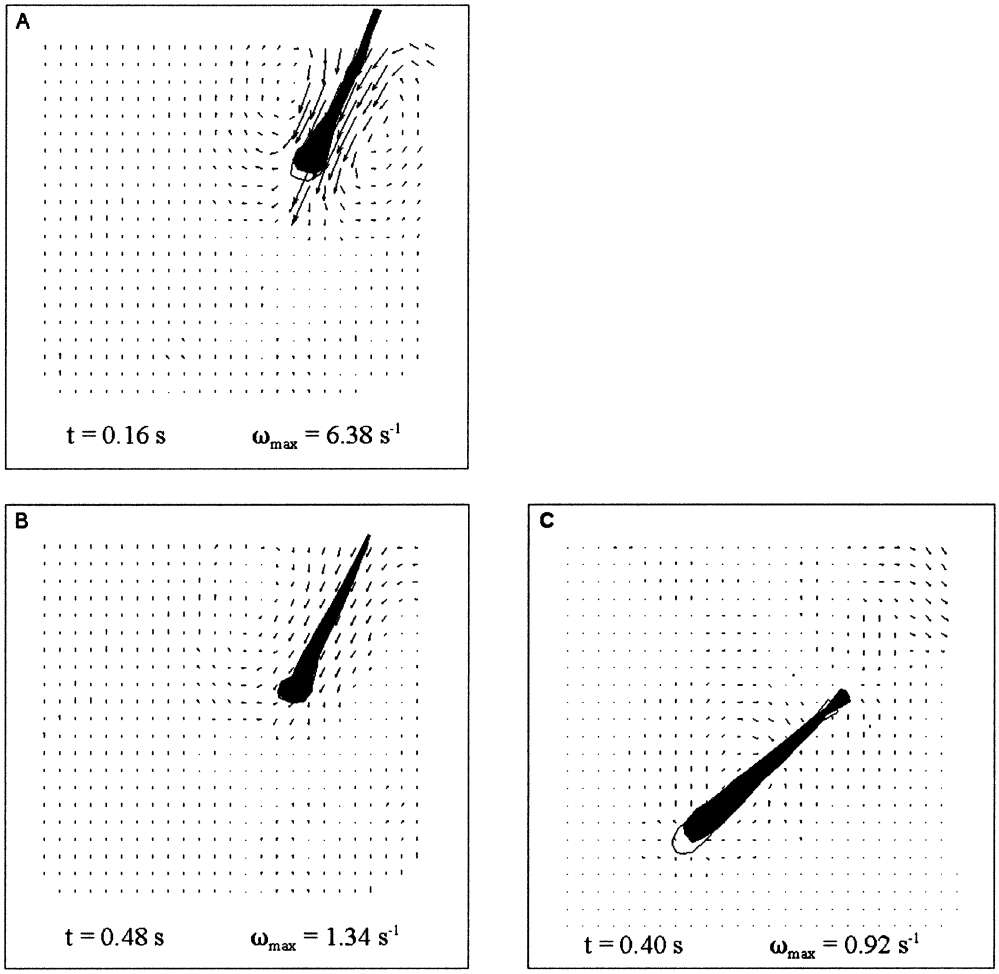

FIG. 6 (panels A and B). Velocity vectors and the maximum vorticity around a coasting 4.1 mm zebra danio larva. The open outline is 0.04 sec after the filled fish drawing. Panel C: The flow field around a coasting 35 mm long adult zebra danio.

ly present. The spacing between the vortices matches the tail beat amplitude and stride length of the swimming sequence. The vortices were shed at the tail tip each time the tail reached its maximum lateral excursion and changed direction. The vorticity reaches a maximum value of 20 sec^{-1} in the center of vortex 1, indicated in Figure 8B.

The total time span or age of the wake is 1.7 sec. The vorticity and the velocities in the vortices and the jet decrease towards the right in Figure 8C. The highest velocity is 91 mm sec^{-1}, which is found near the position of vortex 2. The width of the wake of about 80 mm looks constant over the distance shown. No displacement of vortices can be detected in this wake recording. The center of the rightmost vortex of Figure 8C is most difficult one to detect. We speculate that the wake would no longer be detectable from natural water movements after about 3 sec.

DISCUSSION

The size of the flow fields around different stages of copepods is in the order of the magnitude of their body length. Large magnification is required to observe the moving particles. A small field of view in combination with fast movements makes tethering unavoidable. The animals are moving water past their bodies instead of moving through the water. The amount of water involved is significantly larger in the tethered situation (Emlet, 1990; Gallager, 1993). During foraging, copepods use gravity to increase the entrained amount of water (Strickler, 1982). The fact that tethered animals are not in a position to make use of gravity could provide some compensation for the increase of entrained water due to tether. Although the flow morphology may be somewhat affected, the recordings reveal important information regarding the nature of the flow at low *Re* numbers. This effect will be very limited for the flow fields measured around foraging animals. Indeed estimates of *Re* numbers of free swimming N6 and C1 range between 0.25 and 0.45 (Van Duren and Videler, 1995). However the *Re* number estimates for freely escaping nauplii are considerably higher than *Re* numbers based on the flow past tethered animals. Freely escaping N6 reach *Re* numbers around an average of 11 and C1 average around 7 (with occasional maxima of up to 11). The

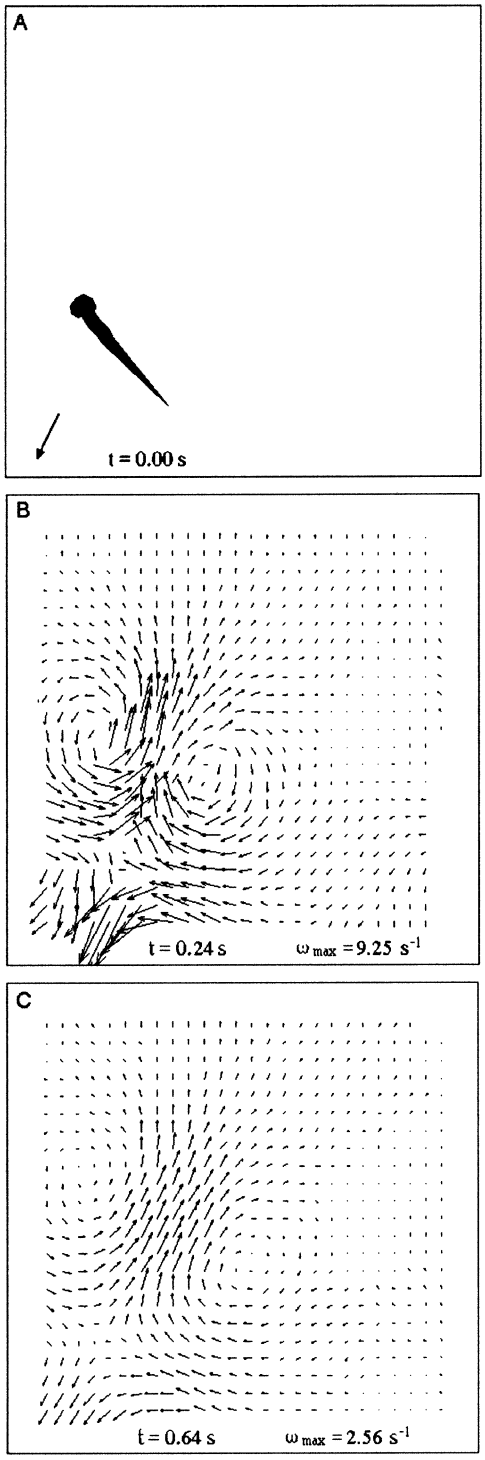

FIG. 7. The wake behind a 4.1 mm zebra danio larva after a tail flick at t = 0 in A where the arrow indicates the swimming direction of the larva. B and C are velocity fields (black arrows) and maximum vorticity at t = 0.24 and t = 0.64 sec after the tail flick respectively.

feeding currents of N6 and C1 are virtually identical despite the large differences in morphology.

The comparison of examples of the escape responses of N6 and C1 at *Re* numbers of 2 and 7, respectively, provides important information about the transition from viscosity to inertia dominated flow. The nauplius basically walks through the water, pushing itself off against the viscous medium which starts to rotate. At higher *Re* numbers, forward momentum is provided by a jet of water through a vortex ring. The size of the ring is several times larger than the animal. Inertia is the important physical factor in his type of hydrodynamic interaction. The change of morphology from nauplius to copepodid does not increase the maximum escape speed, but it probably increases the efficiency and hence diminishes the energetic costs of this important behavior.

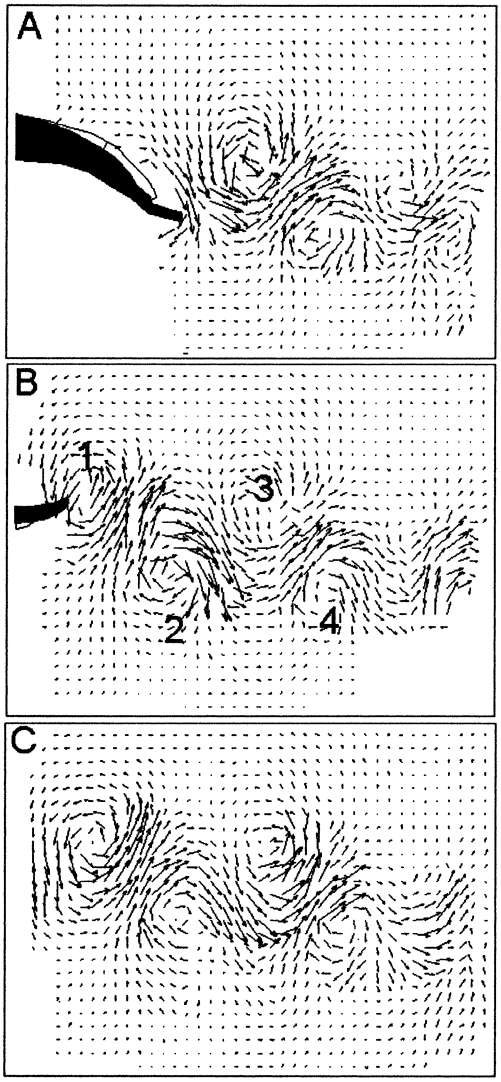

FIG. 8. The wake behind a steadily swimming 12.6 cm long mullet. A–C is a time sequence of the wake velocities (black arrows). A: t = 0 sec; B: t = 0.16 sec; C: t = 0.32 sec. See text for further explanation.

Small fish larvae pay a high drag penalty when they try to coast. The initial *Re* number seems high enough to expect moderate viscous effects, but the substantial speed decrease due to the large volume of entrained water tells a different story. The decrease in speed rap-

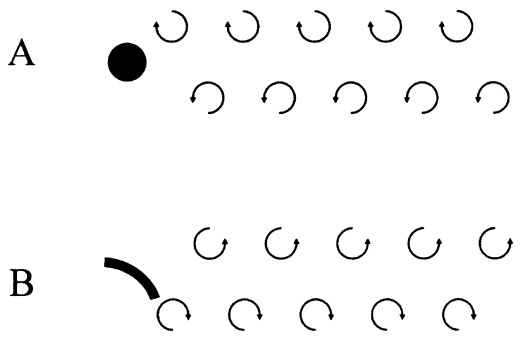

FIG. 9. Schematic drawings of flow patterns in horizontal sections through typical wakes. A. The von Karman vortex street as a result of drag experienced by the flow passing a bluff body. B. An inverse von Karman wake generated by a thrusting plate in left-right flapping motion.

idly increases the drag due to the increasing influence of viscous effects. A coasting adult produces a completely different flow operating in a *Re* regime in the order of multiples of 10^3. Elevated flow velocities of small amounts of water are mainly found in the wake. The pattern is typical for streamlined bodies at higher *Re* numbers (Prandtl and Tietjens, 1957). Small fish larvae can only coast over distances of less than their body length. Adults can cross several body lengths during a glide but usually choose to initiate another burst before their speed has decreased to half the value at the start of the glide. Weihs (1974 and 1980) and Videler and Weihs (1982) deal with the kinematic details and the energetic consequences of burst-and-coast swimming of larval and adult fish.

The flow pattern caused by the tail flick of the 4 mm zebra danio larva is a vortex ring with a jet through the center. The larva is obviously capable of using inertial effects to generate momentum for the escape movement. The size of vortex ring is about the size of the body length of the fish. This is relatively small compared to the size of the ring produced by the escaping copepodid at $Re = 7$, but large compared to the size of the rings in the chain behind the mullet where the diameter of the ring is approximately 0.1 L.

The vortex chain of the mullet is induced by the thrust forces generated by the animal in interaction with the water. The wake structure is interpreted as a horizontal section through a chain of interconnected vortex rings. The rotations and jet direction of such a thrust wake are opposite that of a ''von Karman'' vortex street (Lighthill, 1975), which is the drag induced vorticity pattern behind a stationary cylinder in a flow (the difference is illustrated in Fig. 9). A 3-D impression of a thrust wake behind a fish is given in Figure 10. The stop-start vortices of the tail fin are connected by vortices shed at the dorsal and ventral tail tip during the crossings from side to side. These tail fin tip vortices have been interpreted to be analogous to wing tip vortices of aircraft (Videler, 1993). Although inertia is the dominating factor in the interaction between the mullet and water, farther from the mullet and into the wake, viscosity effects become more dominant, thereby decreasing the flow velocities and reducing the lifespan of the wake.

At higher *Re* numbers the lifespan of wakes is clearly increased. This is well supported by hydrodynamic theory (Visser, 2001). Potentially, these wakes could be perceived and traced by predators. For juvenile copepods that are often preyed upon by mechanoreceptive predators, such as other copepods, this risk is quite considerable. For fish this problem is presumably less significant, since they tend to be hunted by visual predators. However, juvenile fish are known to modify their swimming behavior to reduce water deformation in front of them, when they are preparing to attack copepod nauplii and copepodids, to avoid being detected (Kiørboe and Visser, 1999).

CONCLUSION

The interactions between animals and water are highly dependent on scale effects expressed by the *Re* number. At the lower end of the range ($Re < 1$) water movements are dominated by viscosity. Foraging nauplii and copepodids of *Temora longicornis* rotate water slowly at velocities around 1 mm sec^{-1} close to the moving appendages. At intermediate regimes ($Re > 1$

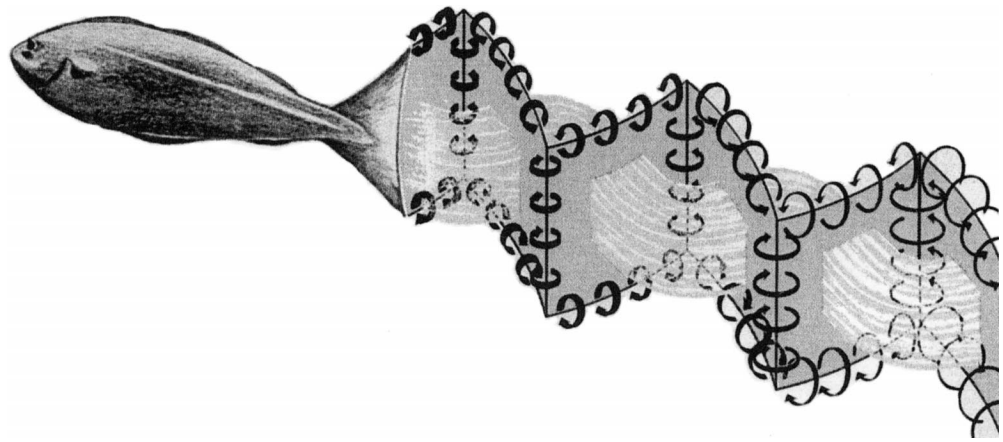

FIG. 10. A 3-D impression of the wake behind a steadily swimming fish (Videler, 1993).

and <7) rotational flows result in the development of vortex rings with a jet through the centre. Due to inertial effects, these structures show up behind adult copepods during escape responses at $Re = 7$. Viscosity brings the rotation of the ring structures to a halt within less than 0.2 sec. Vortex rings with a jet trough the centre become more persistent with increasing *Re* numbers. The flow around coasting and swimming fish larvae and small adults illustrates how inertial effects start to dominate the events. Steadily swimming adult fish of about 10 cm body length ($Re > 10^4$) produce a trail consisting of a chain of interconnected vortex rings with an undulating jet trough the centres of the rings. Trails persist during several seconds after the fish has left. The complexity of the flow in 3 dimensions increases with increasing *Re* number regimes. Future work on inertia dominated flow patterns requires quantitative 3-dimensional flow-visualization techniques.

ACKNOWLEDGMENTS

We thank Malcolm Gordon, Ian Bartol and Jay Hove for the kind invitation to present our work at the symposium on the dynamics and energetics of animal swimming and flying.

REFERENCES

Emlet, R. B. 1990. Flow fields around ciliated larvae: Effects of natural and artificial tethers. Mar. Ecol. Progr. Ser. 63:211–225.

Fuiman, L. A. and P. W. Webb. 1988. Ontogeny of routine swimming activity and performance in zebra danios (Teleostei: Cyprinidae). Anim. Beh. 36:250–261.

Gallager, S. M. 1993. Hydrodynamic disturbances produced by small zooplankton: Case study for the veliger larva of a bivalve mollusc. J. Plankton Res. 15:1277–1296.

Kiørboe, T. and A. W. Visser. 1999. Predator and prey perception in copepods due to hydromechanical signals. Mar. Ecol. Progr. Ser. 179:81–95.

Lighthill, M. J. 1986. *An informal introduction to theoretical fluid mechanics.* Clarendon Press, Oxford.

Lighthill, M. J. 1975. *Mathematical biofluiddynamics.* SIAM, Philadelphia.

Müller, U. K., B. L. E. v. d. Heuvel, E. J. Stamhuis, and J. J. Videler. 1997. Fish foot prints: Morphology and energetics of the wake behind a continuously swimming mullet (*Chelon labrosus* Risso). J. Exp. Biol. 200:2893–2906.

Müller, U. K., J. Smit, E. J. Stamhuis, and J. J. Videler. 2001. How the body contributes to the wake of undulatory fish swimming: Flow fields of a swimming eel (*Anguilla anguilla*). J. Exp. Biol. 204:2751–2762.

Müller, U. K., E. J. Stamhuis, and J. J. Videler. 2000. Hydrodynamics of unsteady fish swimming and the effects of body size: Comparing the flow fields of fish larvae and adults. J. Exp. Biol. 203:193–206.

Prandtl, L. and O. G. Tietjens. 1957. *Applied hydro- and aerodynamics.* Dover publications, Inc., New York.

Reynolds, O. 1883. An experimental investigation of the circumstances which determine whether the motion of water shall be direct or sinuous, and of the law of resistance in parallel channels. Phil. Trans. 174:935–982.

Stamhuis, E. J. and J. J. Videler. 1995. Quantitative flow analysis around aquatic animals using laser sheet particle image velocimetry. J. Exp. Biol. 198:283–294.

Strickler, J. R. 1982. Calanoid copepods, feeding currents and the role of gravity. Science 218:158–160.

Van Duren, L. A. 2000. *Moving* (*in*) *water: Behavioural kinematics, hydrodynamics and energetics of the calanoid copepod Temora longicornis.* Ph.D. thesis, Groningen University.

Van Duren, L. A. and J. J. Videler. 1995. Swimming behaviour of developmental stages of the calanoid copepod *Temora longicornis* at different food concentrations. Mar. Ecol. Progr. Ser. 126:153–161.

Videler, J. J. 1993. *Fish swimming.* Chapman and Hall, London.

Videler, J. J. and D. Weihs. 1982. Energetic advantages of burst and coast swimming of fish at high speeds. J. Exp. Biol. 97:169–178.

Visser, A. W. 2001. Hydromechanical signals in the plankton. Mar. Ecol. Progr. Ser. 222:1–24.

Weihs, D. 1974. Energetic advantages of burst swimming of fish. J. Theor. Biol. 48:215–229.

Weihs, D. 1980. Energetic significance of changes in swimming modes during growth of larval anchovy, *Engraulis mordax.* Fishery Bulletin 77:597–604.